Physics Letters B 689 (2010) 28–35

Contents lists available at ScienceDirect

Physics Letters B

www.elsevier.com/locate/physletb

Probing the Majorana nature of TeV-scale radiative seesaw models at collider experiments

Mayumi Aoki [a], Shinya Kanemura [b,*]

[a] Department of Physics, Tohoku University, Aramaki, Aoba, Sendai, Miyagi 980-8578, Japan
[b] Department of Physics, University of Toyama, 3190 Gofuku, Toyama 930-8555, Japan

ARTICLE INFO

Article history:
Received 4 January 2010
Received in revised form 20 March 2010
Accepted 12 April 2010
Available online 15 April 2010
Editor: T. Yanagida

Keywords:
Radiative seesaw models
Higgs physics
Flavor physics

ABSTRACT

A general feature of TeV-scale radiative seesaw models, in which tiny neutrino masses are generated via loop corrections, is an extended scalar (Higgs) sector. Another feature is the Majorana nature; e.g., introducing right-handed neutrinos with TeV-scale Majorana masses under the discrete symmetry, or otherwise introducing some lepton number violating interactions in the scalar sector. We study phenomenological aspects of these models at collider experiments. We find that, while properties of the extended Higgs sector of these models can be explored to some extent, the Majorana nature of the models can also be tested directly at the International Linear Collider via the electron–positron and electron–electron collision experiments.

1. Introduction

The neutrino data show that neutrinos have tiny masses as compared to the electroweak scale. This is clear evidence for physics beyond the standard model (SM). The data also indicate that the structure of flavor mixing for neutrinos is largely different from that for charged leptons. These facts would suggest that, while charged leptons have Dirac type masses, the neutrino masses are of the Majorana type. The tiny Majorana masses of left-handed neutrinos are generated from the dimension five effective operators

$$\mathcal{L} = \frac{c_{ij}}{2\Lambda}\overline{\nu^c}^i_L \nu^j_L \phi^0 \phi^0, \tag{1}$$

where Λ represents a mass scale, c_{ij} are dimensionless coefficients, and ϕ^0 is the Higgs boson. After electroweak symmetry breaking, the mass matrix M_ν^{ij} for left-handed neutrinos appears as $M_\nu^{ij} = c_{ij}\langle\phi^0\rangle^2/\Lambda$. As the vacuum expectation value (VEV) $\langle\phi^0\rangle$ of the Higgs boson is $\mathcal{O}(100)$ GeV, the observed tiny neutrino masses ($M_\nu^{ij} \lesssim 0.1$ eV) are realized when $(c_{ij}/\Lambda) \sim \mathcal{O}(10^{-14})$ GeV^{-1}. It has been an interesting problem how we can naturally explain such a small number with less fine tuning.

If the operators in Eq. (1) appear at the tree level in the low energy effective theory, Λ has to be as large as $\mathcal{O}(10^8)$–$\mathcal{O}(10^{14})$ GeV for c_{ij} being $\mathcal{O}(10^{-6})$–$\mathcal{O}(1)$ to describe the data. For example, in the tree-level seesaw scenario where right-handed neutrinos are introduced, their Majorana masses have to be set much higher than the electroweak scale [1], corresponding to the scale Λ in Eq. (1). Although the scenario is simple, it requires another hierarchy between the mass of right-handed neutrinos and the electroweak scale, and in addition, physics at such a large mass scale is difficult to be tested at collider experiments.

Quantum generation of neutrino masses is an alternative way to obtain $(c_{ij}/\Lambda) \sim \mathcal{O}(10^{-14})$ GeV^{-1}. Due to the loop suppression factor, Λ in these models can be lower as compared to that in the tree-level seesaw models. Consequently, the tiny neutrino masses would be explained in a natural way by the TeV-scale dynamics without introducing very high mass scales. The original model of this line was proposed by Zee [2], where neutrino masses were generated at the one-loop level. Some variations were considered [3–7], for example, by Zee and Babu [3], Krauss, Nasri and Trodden [4], Ma [5], and the model in Ref. [6]. The last three models contain dark matter (DM) candidates with the odd quantum number under the discrete Z_2 symmetry. It must be a charming point in these TeV-scale radiative seesaw models that they are directly testable at the collider experiments such as Large Hadron Collider (LHC) and the International Linear Collider (ILC).

A general feature in radiative seesaw models is an extended Higgs sector, whose detail is strongly model dependent. The discovery of these extra Higgs bosons and detailed measurements of their properties at current and future collider experiments can give partial evidence for the radiative seesaw models. In the literature [8–14], phenomenology of these radiative seesaw models

* Corresponding author.
E-mail addresses: mayumi@tuhep.phys.tohoku.ac.jp (M. Aoki), kanemu@sci.u-toyama.ac.jp (S. Kanemura).

0370-2693
doi:10.1016/j.physletb.2010.04.024

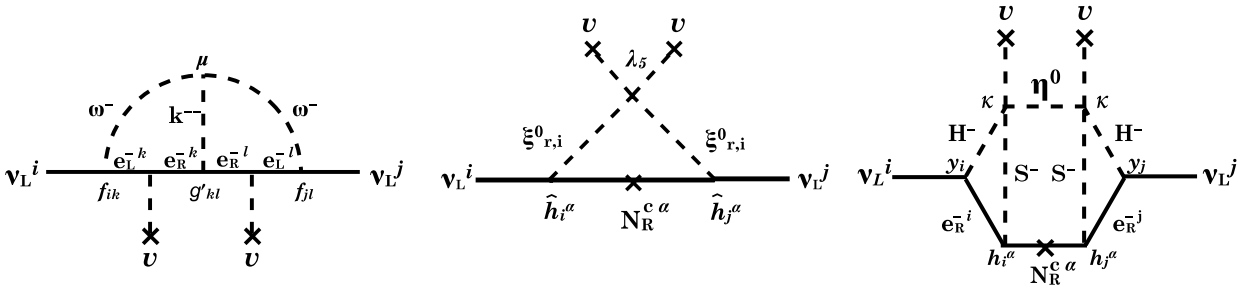

Fig. 1. Feynman diagrams for neutrino masses in the model by Zee and Babu [3] (left), that by Ma [5] (center) and that in Ref. [6] (right).

has already been studied extensively. Such previous works mainly discuss constraints on the flavor structure from the current data for such as neutrino physics and DM, and also study collider phenomenology of the Higgs sectors [15–17,19–24].

Another common feature in radiative seesaw models is the Majorana nature. In order to induce tiny Majorana masses for left-handed neutrinos, we need to introduce its origin such as lepton number violating interactions in the scalar sector [2,3] or right-handed neutrinos with TeV-scale Majorana masses [4–6]. When the future data would indicate an extended Higgs sector predicted by a specific radiative seesaw model, the direct detection of the Majorana property at collider experiments should be a fatal probe to identify the model.

In this Letter, we study the phenomenology in TeV-scale radiative seesaw models, in particular, a possibility of detecting the Majorana nature at collider experiments. We mainly discuss three typical radiative seesaw models as reference models; the model by Zee and Babu where neutrino masses are generated at the two-loop level [3], that by Ma with one-loop neutrino mass generation [5], and that in Ref. [6] where neutrino masses are generated at the three-loop level. Typical parameter regions where the data can be satisfied have been already studied in each model in the literature. We here study collider phenomenology in such typical parameter regions in each model, and discuss the discrimination of these models by measuring the details of the Higgs sector and the Majorana nature at the LHC and the ILC.

2. Radiative seesaw models

2.1. The Zee–Babu model

In the model proposed in Ref. [3] (we refer to as the Zee–Babu model), in addition to singly-charged singlet scalar bosons $\omega^{\pm}$, doubly-charged singlet scalar fields $k^{\pm\pm}$ are introduced, both of which carry the lepton number of two-unit, and their interactions are given by

$$\mathcal{L}_{\rm int} = f_{ab}\big(\overline{L^{ci}_{aL}} L^{j}_{bL}\big)\epsilon_{ij}\omega^{+} + g'_{ab}\big(\overline{\ell^{c}_{aR}}\ell_{bR}\big)k^{++} - \mu k^{++}\omega^{-}\omega^{-} + \text{H.c.}, \tag{2}$$

where L_L is the left-handed lepton doublet and ℓ_R is the right-handed lepton singlet. The matrices f_{ij} and g'_{ab} are respectively an anti-symmetric and a symmetric couplings and the lepton number is violated by the interaction with the parameter μ.

The neutrino mass matrix is generated at the two-loop level via the diagram in Fig. 1 (left);

$$M^{\nu}_{ij} = \sum_{k,\ell=1}^{3}\left(\frac{1}{16\pi^2}\right)^2 \frac{4\mu}{m^2_{\omega}} f_{ik}(y_{\ell_k} g_{k\ell} y_{\ell_\ell}) f_{\ell j} v^2 I_1\big(m^2_k/m^2_{\omega}\big), \tag{3}$$

where y_i $[=\sqrt{2}m_i/v$ $(i = e,\ \mu,\ \tau)]$ are the SM Yukawa coupling constants of charged leptons with the masses m_i and the VEV v ($\simeq 246$ GeV), g_{ij} are defined as $g_{ii} = g'_{ii}$ and $g_{ij} = 2g'_{ij}$ $(i \neq j)$, m_{ω} and m_k are masses of $\omega^{\pm}$ and $k^{\pm\pm}$, and

$$I_1(r) = -\int_0^1 dx \int_0^{1-x} dy \frac{1}{x + (r-1)y + y^2} \ln\frac{y(1-y)}{x + ry}, \tag{4}$$

where $I_1(r)$ takes the value of around 3–0.2 for $10^{-2} \lesssim r \lesssim 10^2$. The universal scale of neutrino masses is determined by the two-loop suppression factor $1/(16\pi^2)^2$ and the lepton number violating parameter μ. The charged lepton Yukawa coupling constants y_{ℓ_i} $(y_e \ll y_{\mu} \ll y_{\tau} \lesssim 10^{-2})$ give an additional suppression factor. Thus, any of f_{ij} or g_{ij} can be of $\mathcal{O}(1)$ when m_{ω} and m_k are at the TeV scale. The flavor structure of the mass matrix is determined by the combination of the coupling constants f_{ij} and $y_i g_{ij} y_j$.

The flavor off-diagonal coupling constants f_{ij} and g_{ij} induce lepton flavor violation (LFV). From the results of $\mu \to e\gamma$, $\tau \to e\gamma$ and $\tau \to \mu\gamma$, $|f_{\mu\tau} f_{\tau e}|$, $|f_{\tau\mu} f_{\mu e}|$ and $|f_{\tau e} f_{e\mu}|$ are respectively constrained as a function of m_{ω}. The data of rare decays of $\mu \to eee$, $\tau \to \mu\mu e$ and $\tau \to \mu ee$ are also used to constrain the combinations $|g_{\mu e} g_{ee}|$, $|g_{\tau e} g_{\mu\mu}| + |g_{\tau\mu} g_{\mu e}|$ and $|g_{\tau e} g_{\mu e}| + |g_{\tau\mu} g_{ee}|$, respectively, depending on m_k. The $g-2$ data can also be used to constrain a combination of these coupling constants with m_{ω} and m_k.[1]

In the scenario with hierarchical neutrino masses, f_{ij} satisfy $f_{e\mu} \simeq f_{e\tau} \simeq f_{\mu\tau}/2$. The typical relative magnitudes among the coupling constants g_{ij} can be $g_{\mu\mu} : g_{\mu\tau} : g_{\tau\tau} \simeq 1 : m_{\mu}/m_{\tau} : (m_{\mu}/m_{\tau})^2$. For $g_{\mu\mu} \simeq 1$, the neutrino data and the LFV data give the constraints such as $m_k \gtrsim 770$ GeV and $m_{\omega} \gtrsim 160$ GeV [10]. On the other hand, the constraints on the couplings and masses are more stringent for the inverted neutrino mass hierarchy. The current data then gives $m_{\omega} \simeq 825$ GeV for $g_{\mu\mu} \simeq 1$ [10]. One of the notable things in this case is the lower bound on $\sin^2 2\theta_{13}$, which is predicted as around 0.002 [9].

2.2. Models with TeV-scale right-handed neutrinos with a discrete Z_2 symmetry

Similar to the tree-level seesaw model, tiny masses of left-handed neutrinos would also come from Majorana masses $M_{N^{\alpha}_R}$ of gauge-singlet right-handed neutrinos N^{α}_R in the radiative seesaw scenario [4–6]. One simple way to realize the absence of the tree-level Yukawa interaction $\bar{\nu}^i_L \tilde{\Phi} N^{\alpha}_R$ is introduction of a discrete Z_2 symmetry, with the assignment of the odd quantum number to N^{α}_R and the even to the SM particles. To obtain the dimension five operator in Eq. (1) at the loop level, we need to introduce additional Z_2-odd scalar fields. The lightest of all the Z_2-odd particles can be a candidate of DM if it is electrically neutral. The

[1] If we take $g_{ee} = 0$, then m_k is unbounded from the $\mu \to eee$ and $\tau \to \ell ee$ results ($\ell = e$ or μ), so that relatively light $k^{\pm\pm}$ ($m_k \sim 100$–200 GeV) are possible.

original model of the radiative seesaw model with such a discrete symmetry is proposed by Krauss, Nasri, and Trodden [4], in which neutrino masses are induced at the three-loop level. In the following, we consider two variant models of the Krauss–Nasri–Trodden (KNT) model.

2.2.1. The Ma model

The model in Ref. [5], which we here refer to as the Ma model, is the simplest radiative seesaw model with right-handed neutrinos N_R^α, in which the discrete Z_2 symmetry is introduced and its odd quantum number is assigned to N_R^α. The Higgs sector is composed of two Higgs doublet fields, one of which (Ξ) is Z_2 odd. As long as the Z_2 symmetry is exact, the neutral components of Ξ do not receive VEVs. We have one SM-like Higgs boson h, and four physical Z_2-odd scalar states; ξ_r^0 (CP-even), ξ_i^0 (CP-odd) and $\xi^\pm$ as physical scalar states. This Z_2 odd Higgs doublet is sometimes called as the inert Higgs doublet [15] or the dark scalar doublet [17]. The LEP II limits are studied in this model in Ref. [18].

The neutrino masses are generated at the one loop level via the diagram depicted in Fig. 1 (center), in which Z_2 odd particles, ξ^0 and N_R^α, are in the loop. The mass matrix is calculated as

$$M_{ij}^\nu = -\sum_{\alpha=1}^{3}\left(\frac{1}{16\pi^2}\right)\frac{\hat{h}_i^\alpha \hat{h}_j^\alpha \lambda_5 v^2}{M_{N_R^\alpha}}\frac{1}{1-r^\alpha}\left(1+\frac{1}{1-r^\alpha}\ln r^\alpha\right), \quad (5)$$

where $\hat{h}_i^\alpha$ are the Yukawa coupling constants of $\bar{\nu}_L^i \tilde{\Xi} N_R^\alpha$, $M_{N_R^\alpha}$ is the Majorana mass of the α-th generation right-handed neutrino N_R^α, $\lambda_5 = (m_{\xi_i}^2 - m_{\xi_r}^2)/v^2$, $r^\alpha = m_0^2/M_{N_R^\alpha}^2$ with $m_0 = (m_{\xi_i} + m_{\xi_r})/2$, where m_{ξ_r} and m_{ξ_i} are masses of ξ_r^0 and ξ_i^0, respectively. The universal scale for neutrino masses is determined by the one-loop suppression factor $1/(16\pi^2)$, λ_5 and $M_{N_R^\alpha}$. The flavor structure in M_{ij}^ν is realized by the combination of $\hat{h}_i^\alpha \hat{h}_j^\alpha / M_{N_R^\alpha}$. Therefore, for $M_{N_R^\alpha} \sim \mathcal{O}(1)$ TeV, the combination of the coupling constants would be $|\lambda_5|(\hat{h}_i^\alpha)^2 \sim 10^{-9}$.

In this model, there are two scenarios with respect to the DM candidate; i.e., the lightest right-handed neutrino N_R^1 or the lightest Z_2-odd neutral field (ξ_r^0 or ξ_i^0). For both cases, there are parameter regions where the neutrino data are adjustable without contradicting other phenomenological constraints [13]. In this Letter, we consider the case where the dark doublet component ξ_r^0 is the DM candidate.[2] When the mass of the DM is around 50 GeV, the typical value of $\lambda_5 \sim 10^{-2}$ for the neutrino masses gives the mass difference between ξ_r^0 and ξ_i^0 about 10 GeV.[3] The relic abundance of such DM is consistent with the WMAP data [19].

2.2.2. The AKS model

In the model in Ref. [6], which we here refer to as the AKS model, it is intended that not only the tiny neutrino masses and DM but also baryon asymmetry of Universe are explained at the TeV scale. In addition to the TeV-scale right-handed neutrinos N_R^α ($\alpha = 1, 2$), the Higgs sector is composed of Z_2-even two Higgs doublets Φ_i ($i = 1, 2$) and Z_2-odd charged singlets $S^\pm$ and a Z_2-odd neutral real singlet η^0. Therefore the physical states in the Z_2-even sector are H (CP-even), A (CP-odd), $H^\pm$ and h (CP-even).

The neutrino mass matrix is generated at the three-loop level via the diagram in Fig. 1 (right), and is expressed as

$$M_{ij}^\nu = \sum_{\alpha=1}^{2}\left(\frac{1}{16\pi^2}\right)^3 \frac{(y_{\ell_i} h_i^\alpha)(y_{\ell_j} h_j^\alpha)(\kappa \tan\beta)^2 v^2}{M_{N_R^\alpha}} \times I_2(m_{H^\pm}, m_{S^\pm}, m_{N_R^\alpha}, m_\eta), \quad (6)$$

where $m_{H^\pm}$, $m_{S^\pm}$, $m_{N_R^\alpha}$ and m_η are the masses of the doublet originated charged Higgs boson $H^\pm$, $S^\pm$, N_R^α and η^0, respectively; h_i^α and κv are the coupling constants of $\bar{N}_R^\alpha e_R^i S^+$ and $H^+ S^- \eta^0$, respectively; $\tan\beta = \langle\Phi_2^0\rangle/\langle\Phi_1^0\rangle$, and

$$I_2(x, y, z, w) = \frac{-4z^2}{z^2 - w^2}\int_0^\infty u\,du\left\{\frac{B_1(-u; x, y) - B_1(-u; 0, y)}{x^2}\right\}^2 \times \left(\frac{z^2}{u+z^2} - \frac{w^2}{u+w^2}\right), \quad (7)$$

where B_1 is the tensor coefficient function in the Passarino–Veltman's formalism [25]. Although the Higgs sector is rather complicated to make it possible for the electroweak baryogenesis scenario, the flavor structure is determined only by the combination of h_i^α and $m_{N_R^\alpha}$ just as in the Ma model. The mass matrix has the three loop factor $1/(16\pi^2)^3$ with additional suppression factor by y_i. They are enough to reproduce the neutrino mass scale. Thus, the electron associated coupling constants $h_e^{1,2}$ and the scalar coupling κ are of $\mathcal{O}(1)$ for $m_{N_R}^{1,2} \sim \mathcal{O}(1)$ TeV. The Yukawa coupling constants h_i^α are hierarchical as $h_e^{1,2}$ ($\simeq \mathcal{O}(1)$) $\gg h_\mu^{1,2} \gg h_\tau^{1,2}$.

The parameter sets which satisfy the current data from neutrino oscillation, LFV, relic abundances of DM and the condition for strongly first order electroweak phase transition are studied in Refs. [6,14]. To reproduce the neutrino data, the mass of $H^\pm$ should be 100–200 GeV. This is an important prediction of the model. In order to avoid the constraint from $b \to s\gamma$, the Yukawa interaction for the doublet fields takes the form of so-called Type-X [20],[4] where only one of the doublets couples to leptons and the rest does to quarks. The physics of the Type-X two Higgs doublet model (THDM) shows many distinctive features from the other type of extended Higgs sectors. For example, H and A decay mainly into $\tau^+\tau^-$ when $\tan\beta \gtrsim 3$ and $\sin(\beta-\alpha) \simeq 1$ [20]. There are basically two DM candidates, η^0 and N_R^α. The mass of $S^\pm$ is strongly constrained by the current data and the requirement for strongly first order phase transition [6,14]. The coupling constant of S^+S^-h is required to be of $\mathcal{O}(1)$, whose indirect effect appears in the quantum correction to the hhh coupling constant as a large deviation from the SM prediction [14,28]. As long as kinematically allowed, $S^\pm$ decays via $S^\pm \to H^\pm\eta^0$ by 100%.

3. Phenomenology in radiative seesaw models at the LHC

The existence of the extra Higgs bosons such as charged scalar bosons, which are a common feature of radiative seesaw models, can be tested at the LHC. Details of the properties of such extra Higgs bosons are strongly model dependent, so that we can distinguish models via detailed measurements of extra Higgs bosons. In addition, as the (SM-like) Higgs boson h is expected to be detected, its mass and decay properties are thoroughly measured [29]. The radiative seesaw models with a DM candidate can also be indirectly tested via the invisible decay of h as long as its branching ratio is more than about 25% for $m_h = 120$ GeV with $\mathcal{L} = 30$ fb^{-1} [30]. The phenomenological analyses at the LHC in each model are in the literature [9–12,14,16,17,20–24]. We here review some remarkable features.

[2] In Ref. [13], the scenario where the lightest right-handed neutrino is DM is explored.

[3] In order to avoid constraint from the DM direct search results, it is required that $|\lambda_5| > 10^{-6}$.

[4] Type-X is referred to as Type-IV in Ref. [26] and Type-I' in Ref. [27].

At the LHC, $\omega^\pm$ and $k^{\pm\pm}$ in the Zee–Babu model can be produced in pair, via the Drell–Yan s-channel processes $q\bar{q} \to \omega^+\omega^-$ and $q\bar{q} \to k^{++}k^{--}$. The direct detection of $k^{\pm\pm}$ can be a signature for this model. The $\sigma(q\bar{q} \to k^{++}k^{--})$ is around 0.1 fb for $m_k \sim 800$ GeV. If $k^{\pm\pm}$ mainly decay into 4μ (or $4e$), the number of the signal event with $\mathcal{L} = 100$ fb^{-1} [31] is enough for the discovery for $m_k \lesssim 800$ GeV [9]. The doubly-charged Higgs bosons are however also predicted in the models with complex triplet scalar fields, $\Delta = (\Delta^{\pm\pm}, \Delta^\pm, \Delta^0)$. The gauge coupling $W^\pm\Delta^\pm\Delta^{\mp\mp}$ induces the single doubly-charged Higgs production $q\bar{q}' \to W^{\pm *} \to \Delta^{\pm\pm}\Delta^\mp$, whose cross section is comparable to that of $q\bar{q} \to \gamma^*, Z^* \to \Delta^{++}\Delta^{--}$ [32]. The absence of the gauge coupling $W^\pm\omega^\pm k^{\mp\mp}$ is an important distinctive feature of the Zee–Babu model with gauge singlet doubly-charged Higgs bosons from the triplet model. The singly-charged Higgs boson $\omega^\pm$ would be more difficult to see the signal at the LHC because the final state from $\omega^+\omega^-$ is $\ell^+\ell^-$ plus a missing energy.

In the Ma model, if the mass of the DM candidate satisfies $m_{\xi_{r,i}} < m_h/2$, the SM Higgs boson with $m_h \lesssim 2m_W$ decays mainly into the DM pairs [16,17]. For $m_{\xi_r} = 50$ GeV and $m_{\xi_i} = 60$ GeV, the branching ratio of the invisible decay $h \to \xi_r^0\xi_r^0$ reaches to 70% around $m_h \sim 120$ GeV, which can be observed at the LHC. The $h \to \gamma\gamma$ mode is suppressed by an additional contributions from $\xi^\pm$ [17]. In Ref. [17], the discovery potential of the dark scalar doublet is also analyzed by $pp \to \xi_i^0\xi_r^0$ for the benchmark points, $m_{\xi_r} = 50$ GeV, $m_{\xi_i} = 60$–80 GeV, and $m_{\xi^\pm} = 170$ GeV. The decay branching ratio of the CP-odd dark scalar, $\xi_i^0 \to Z^*\xi_r^0 \to \ell\bar{\ell}\xi_r$, is about 0.09 (0.07) for $m_{\xi_i} - m_{\xi_r} = 10$ (30) GeV. A signature $\ell\ell$ plus a missing energy in the benchmark scenario may be discovered by the optimal cuts.

In the AKS model, the invisible decay of the SM-like Higgs boson $h \to \eta^0\eta^0$ can also open if kinematically allowed. For the typical scenario in Refs. [6,14], the branching ratio of the invisible decay can amount to $B(h \to \eta^0\eta^0) \simeq 36$ (34)% for $m_\eta = 48$ GeV, $m_h = 120$ GeV and $\tan\beta = 3$ (10), so it would be testable at the LHC. As the coupling of hS^+S^- is strong, the partial width of $\Gamma(h \to \gamma\gamma)$ deviates from the SM prediction. The lepton specific decays of extra Higgs bosons A, H and $H^\pm$ are discriminative feature of the Type-X THDM [20–24]. The dominant decay mode of $H(A)$ is $H \to \tau^+\tau^-$; $B(H(A) \to \tau^+\tau^-) \simeq 1$ for $\tan\beta \gtrsim 3$. The decay into $\mu^+\mu^-$ is suppressed by a factor of $(m_\mu/m_\tau)^2$. These neutral bosons can be seen by $gg \to h, A, H \to \tau^+\tau^-$ ($\mu^+\mu^-$) [20,22,24]. The doublet originated charged Higgs boson $H^\pm$ (as well as extra neutral ones) is as light as 100–200 GeV, so that the property of the Type-X THDM can also be tested by $pp \to AH^\pm \to \tau^+\tau^-\tau^\pm\nu_\tau$ [20,23] and $pp \to AH \to 4\tau$ [20,21]. On the other hand, the mass of the Z_2-odd charged Higgs bosons $S^\pm$ is around 400 GeV in the typical scenario in Refs. [6,14]. They are produced in pair via the Drell–Yan process, and decay as $S^+S^- \to H^+H^-\eta^0\eta^0 \to \tau^+\tau^-\nu\nu\eta^0\eta^0$. The event rate is about 0.5 fb for $m_{S^\pm} = 400$ GeV when $\tan\beta \gtrsim 2$. Separation of the S^+S^- signal from the H^+H^- event and also the SM backgrounds seems to be challenging.

At the LHC, via the physics of extra scalar bosons such as (singly and/or doubly) charged Higgs bosons and CP-even Higgs bosons, the structure of the extended Higgs sector can be clarified to some extent. In addition, the invisible decay of the SM-like Higgs boson and the mass spectrum of the extra Higgs bosons would give important indication for a possibility to a radiative seesaw scenario. However, although they would be a strong indication of radiative seesaw models, one cannot conclude that such Higgs sector is of the radiative seesaw models. In order to further explore the possibility to such models, we have to explore the other common feature of radiative seesaw models, such as the Majorana nature. In the next section, we discuss a possibility of testing the Majorana nature at ILC experiments.

4. Phenomenology in radiative seesaw models at the ILC

At the ILC, properties of the Higgs sector can be measured with much better accuracy than at the LHC, so that we would be able to reconstruct the Higgs potential in any extended Higgs sector if kinematically accessible. Invisible decays of the Higgs boson can also be tested when the branching ratio $B(h \to \textit{invisible})$ is larger than a few % [33]. Furthermore, the Majorana nature in radiative seesaw models; i.e., the existence of TeV scale right-handed Majorana neutrinos or that of lepton number violating interaction, would also be tested at the ILC.

4.1. Electron–positron collisions

In the pair production of charged scalar bosons at the e^+e^- collision, which appear in the radiative seesaw models ($\omega^+\omega^-$ in the Zee–Babu model, $\xi^+\xi^-$ in the Ma model, and S^+S^- (and H^+H^-) in the AKS model), there are diagrams of the t-channel exchange of left-handed neutrinos or right-handed neutrinos in addition to the usual Drell–Yan type s-channel diagrams. The contribution of these t-channel diagrams is one of the discriminative features of radiative seesaw models, and no such contribution enters into the other extended Higgs models such as the THDM.[5] These t-channel effects show specific dependences on the center-of-mass energy $\sqrt{s}$ in proportion to $\log s$ in the production cross section, and enhances the production rates of the signal events for higher values of $\sqrt{s}$. The final states of produced charged scalar boson pairs are quite model dependent but with missing energies;

$$e^+e^- \to \omega^+\omega^- \to \ell_L^+\ell_L^-\underline{\bar{\nu}_L\nu_L}, \quad \text{[The Zee–Babu model]} \tag{8}$$

$$e^+e^- \to \xi^+\xi^- \to W^{+(*)}W^{-(*)}\xi_r^0\xi_r^0 \to jjjj(jj\ell_L\underline{\nu_L})\underline{\xi_r^0\xi_r^0}, \quad \text{[The Ma model]} \tag{9}$$

$$e^+e^- \to S^+S^- \to H^+H^-\eta^0\eta^0 \to \tau_R^+\tau_R^-\underline{\bar{\nu}_L\nu_L\eta^0\eta^0}, \quad \text{[The AKS model]} \tag{10}$$

where underlined parts in the final states are observed as missing energies.

4.1.1. The Zee–Babu model

In the Zee–Babu model, the decay branching pattern of $\omega^\pm$ is determined by the relative magnitudes of the coupling constants f_{ij}. As a reference scenario, we take a parameter set

$$\begin{aligned} &m_\omega = 300\ \text{GeV}, \quad m_k = 1200\ \text{GeV}, \quad \mu = 800\ \text{GeV}, \\ &f_{e\mu} = f_{e\tau} = 0.013, \quad f_{\mu\tau} = 0.027, \\ &g_{ee} = 0.17, \quad g_{\mu\mu} = 1.8, \quad g_{\tau\tau} = 0.0061, \\ &g_{e\mu} = 5.7 \times 10^{-5}, \quad g_{e\tau} = 0.011, \quad g_{\mu\tau} = -0.081, \end{aligned} \tag{11}$$

which satisfies the neutrino data for the normal mass hierarchy. In this scenario, the rate in final states $\ell^+\ell^- = e^+e^-$, $e^\pm\mu^\mp$, $e^\pm\tau^\mp$, $\mu^+\mu^-$, $\mu^\pm\tau^\mp$, $\tau^+\tau^-$ is given by 2, 13, 13, 19, 36, 19, respectively. In Fig. 2, the differential cross section $d\sigma/d\cos\theta_\mu$ for the

[5] In the minimal supersymmetric standard model (MSSM) selectron pair production can have similar t-channel contributions (the Bino exchange). In such a case, the final state would be something like an e^+e^- pair plus a missing energy. Therefore, we can discriminate it from the radiative seesaw models.

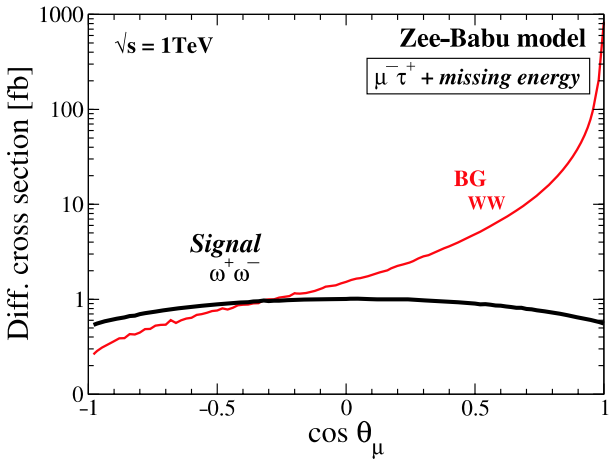

Fig. 2. The differential cross section of $e^+e^- \to \omega^+\omega^- \to \mu^-\tau^+$ (+missing energy) as a function of the angle between the outgoing muon and the beam axis in the Zee–Babu model for $\sqrt{s} = 1$ TeV. The rate of $\mu^-\tau^+$ (+missing energy) from main background $e^+e^- \to W^+W^-$ is also shown.

signal $e^+e^- \to \omega^+\omega^- \to \mu^-\tau^+$ (+missing energy) is shown for $\sqrt{s} = 1$ TeV as a function of $\cos\theta_\mu$, where θ_μ is the angle between the outgoing muon and the beam axis. The main background comes from the W pair production, which is also plotted. The angle cut (e.g. $\cos\theta_\mu < -0.5$) improves the ratio of the signal and the background.[6]

At current and future LFV experiments, the coupling constants f_{ij} and g_{ij} can be further tested via the LFV rare decays such as $\ell \to \ell'\gamma$ and $\ell \to \ell'\ell'\ell''$. The same operators as in $\ell^- \to \ell'^{\mp}e^-e^{\pm}$ would also be tested directly at the ILC via $e^{\pm}e^- \to \ell^-\ell'^{\pm}$. In the scenario in Eq. (11), we estimate that $\sigma(e^+e^- \to \mu^{\pm}\tau^{\mp}) \sim 5$ fb for $\sqrt{s} = 1$ TeV. When we take $g_{ee} = 0.4$, $g_{e\tau} = 0.01$, $m_k = \mu = 1.2$ TeV and $m_\omega = 400$ GeV, which also satisfy all the current data, we obtain $\sigma(e^+e^- \to \tau^{\pm}e^{\mp}) \sim 0.76$ (1.7) fb for $\sqrt{s} = 500$ GeV (1 TeV).

4.1.2. The Ma model

In the Ma model, the coupling constants $\hat{h}^\alpha_e$ $(\alpha = 1, 2)$[7] are strongly constrained from neutrino data and LFV data. As a typical choice of parameters, we consider[8]

$$\begin{aligned} &m_{\xi_r} = 50\ \text{GeV}, \qquad m_{\xi_i} = 60\ \text{GeV}, \\ &m_{\xi^\pm} \sim 100\ \text{GeV}, \qquad m_{N^1_R} = m_{N^2_R} = 3\ \text{TeV}, \\ &\lambda_5 = -1.8 \times 10^{-2}, \quad \hat{h}^\alpha_e,\ \hat{h}^\alpha_\mu,\ \hat{h}^\alpha_\tau \sim 10^{-5}, \end{aligned} \tag{12}$$

in which the normal neutrino mass hierarchy is realized. Because $\hat{h}^\alpha_e$ are very small for a TeV scale $m_{N^\alpha_R}$, the contribution of the t-channel diagrams to the signal $e^+e^- \to \xi^+\xi^-$ is much smaller than that from Drell–Yan type diagrams. For most of the possible values of $\hat{h}^\alpha_\ell$ and $m_{N^\alpha_R}$ which satisfy the LFV and the neutrino data, the contribution of the t-channel diagrams is negligible. The production cross section of a charged Higgs pair $\xi^+\xi^-$ is therefore similar to that in the usual THDM: about 92 (10) fb for $m_{\xi^\pm} = 100$ (150) GeV at $\sqrt{s} = 500$ GeV. The produced $\xi^\pm$ decay into $W^{\pm(*)}\xi^0_{r,i}$.[9]

In Fig. 3 (*left*), we show the invariant mass distribution of the di-jet jj of the production cross section of the signal, $e^+e^- \to \xi^+\xi^- \to W^{+*}W^{-*}\xi^0_r\xi^0_r \to jj\mu\nu\xi^0_r\xi^0_r$ for $m_{\xi^\pm} = 100$ GeV. The main backgrounds come from WW. The $jj\mu\mu$ events from ZZ, $\gamma\gamma$, and $Z\gamma$ can also be the backgrounds. A factor of 0.1 is multiplied to the rate of the $jj\mu\mu$ backgrounds for the miss-identification probability of a muon. The signal is significant around $M(jj) \sim 30$ GeV. The invariant mass cut (such as 15 GeV $< M(jj) <$ 40 GeV) is effective to reduce the backgrounds. For the numerical evaluation, we have used a package CalcHEP 2.5.4 [34].

For $m_{\xi^\pm} > m_W + m_{\xi_r}$, on the other hand, the signal $W^+W^-\xi^0_r\xi^0_r$ can be measured by detecting the events of four jets with a missing energy. The main background comes from $W^+W^-\nu\nu$ and $t\bar{t}$. By the invariant mass cuts of two-jet pairs at the W boson mass, the biggest background from WW can be eliminated. In Fig. 3 (*right*), we show the invariant mass distribution of $jjjj$ of the production cross sections of the signal and the backgrounds without any cut. A factor of 0.1 is multiplied to the rate of tt background, by which the probability of the lepton from a W that escapes from detection is approximately taken into account. The signal is already significant. The invariant mass cut ($M(jjjj) < 300$ GeV) gives an improvement for the signal/background ratio.

4.1.3. The AKS model

For the AKS model, we take a typical successful scenario for the neutrino data with the normal mass hierarchy, the LFV data and the DM data as well as the condition for strongly first order phase transition [6,14];

$$\begin{aligned} &m_\eta = 50\ \text{GeV}, \qquad m_{H^\pm} = 100\ \text{GeV}, \\ &m_{S^\pm} = 400\ \text{GeV}, \qquad m_{N^1_R} = m_{N^2_R} = 3\ \text{TeV}, \\ &h^1_e = h^2_e = 2 \gg h^1_\mu, h^2_\mu \gg h^1_\tau, h^2_\tau, \\ &\kappa \sim \mathcal{O}(1), \qquad \sin(\beta-\alpha) = 1, \qquad \tan\beta = 10. \end{aligned} \tag{13}$$

Because $h^{1,2}_e \sim \mathcal{O}(1)$, the contribution from the t-channel N^α_R exchange diagrams to the production cross section of S^+S^- dominate that from the Drell–Yan diagrams [14]. The cross section is about 87 fb for $m_{S^\pm} = 400$ GeV at $\sqrt{s} = 1$ TeV. As the decay branching ratio of $S^\pm \to H^\pm\eta^0$ is 100% and that of $H^\pm \to \tau^\pm\nu$ is also almost 100% because of the Type-X THDM interaction for $\tan\beta = 10$, the final state of the signal is $\tau^+\tau^-\bar{\nu}\nu\eta^0\eta^0$ with almost the same rate as the parent S^+S^- production. The main SM backgrounds are $\tau^+\tau^-$ and $\tau^+\tau^-\bar{\nu}\nu$. The pair production of the doublet like charged Higgs boson H^+H^- can also be the background. As the signal rate dominantly comes from the t-channel diagram, it becomes larger for larger $\sqrt{s}$, while the main backgrounds except for $\tau\tau\nu_e\nu_e$ are smaller because they are dominantly s-channel processes (Fig. 4 (*left*)). At $\sqrt{s} = 1$ TeV, the rate of the signal without cut is already large enough as compared to those of the backgrounds. It is expected that making appropriate kinematic cuts will improve the signal background ratio to a considerable extent. The $\sqrt{s}$ scan will help us to confirm that the signal rate comes from the t-channel diagrams. Fig. 4 (*right*) shows the differential cross section of the signal at $\sqrt{s} = 1$ TeV as a function of $\cos\theta_{\tau^-}$, where θ_{τ^-} is the angle between the direction of

[6] Although in this Letter we mainly discuss the case where m_k is at the TeV scale, we just comment on the case of lighter $k^{\pm\pm}$. In such case, the pair production of $k^{++}k^{--}$ can be a clear signature of this model, whose signal is the like-sign dilepton pairs with opposite direction [3,9].

[7] Here we consider the minimal case of two generations for the right-handed neutrino.

[8] The relatively large mass difference between $\xi^\pm$ and $\xi^0_{r,i}$ implies a significant deviation from the custodial symmetry in the Higgs sector, which affects the allowed mass m_h of the SM like Higgs boson h. The larger m_h is favored for larger mass difference of $m_{\xi^\pm} - m_{\xi_{r,i}}$.

[9] The $\xi^0_r\xi^0_i$ production can also be interesting. The final state should be two jets (or dilepton) plus a missing energy. The cross section for $e^+e^- \to \xi^0_r\xi^0_i \to \xi^0_r\xi^0_r jj$ is about 40 fb at $\sqrt{s} = 500$ GeV.

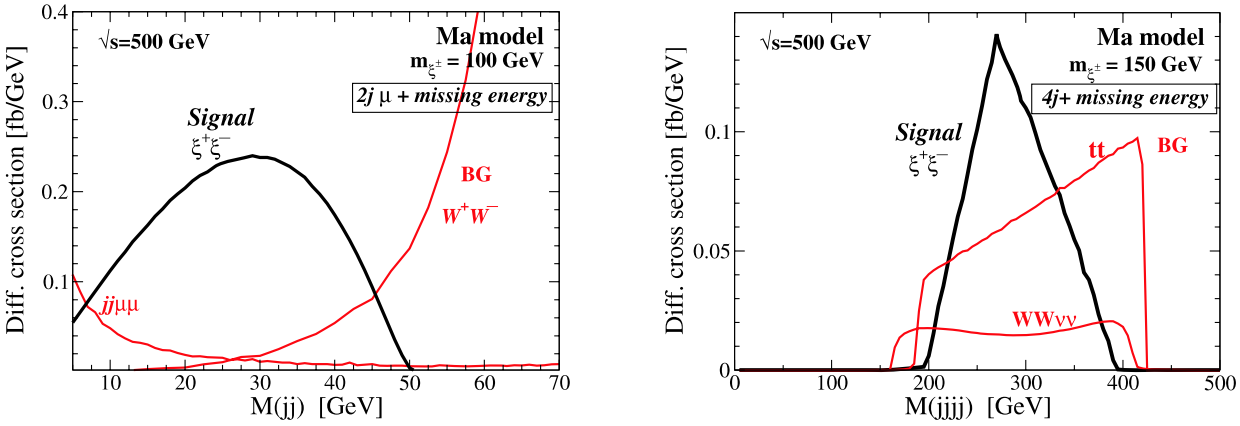

Fig. 3. The jets invariant mass distributions of the production rates of the signal in the Ma model at $\sqrt{s} = 500$ GeV. *Left*: The di-jet invariant mass $M(jj)$ distribution of the signal $e^+e^- \to \xi^+\xi^- \to jj\mu\nu\xi_r^0\xi_r^0$ for $m_{\xi^\pm} = 100$ GeV. *Right*: $M(jjjj)$ distribution of $e^+e^- \to \xi^+\xi^- \to W^+W^-\xi_r^0\xi_r^0 \to jjjj\xi_r^0$ for $m_{\xi^\pm} = 150$ GeV. In addition to the rate from the signal process, those for main backgrounds are also shown.

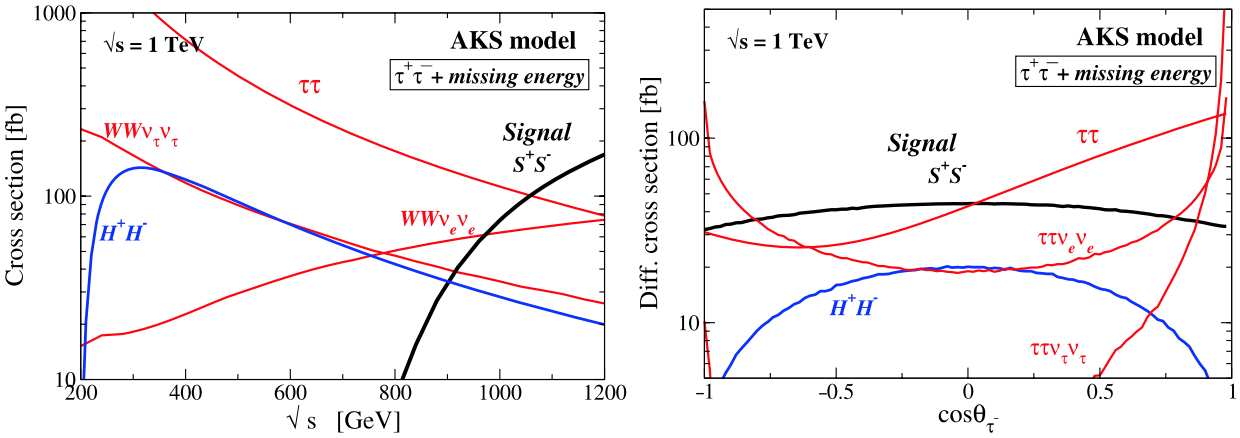

Fig. 4. *Left*: The cross sections of the signal, $e^+e^- \to S^+S^- \to \tau^+\tau^-$ (+ missing energy), in the AKS model as a function of the collision energy $\sqrt{s}$. *Right*: The differential cross section of the signal for $\sqrt{s} = 1$ TeV as a function of the angle of the direction of the outgoing τ^- and the beam axis of incident electrons. In addition to the rate from the signal, those from backgrounds such as $\tau^+\tau^-$, $\tau^+\tau^-\bar{\nu}\nu$ and H^+H^- are also shown.

the outgoing τ^- and the beam axis of incident electrons. The distribution of the background from $\tau\tau$ is asymmetric, so that the angle cut for larger $\cos\theta_{\tau^-}$ reduces the backgrounds.

4.2. Electron–electron collisions

As already stated, the ILC has a further advantage to test radiative seesaw models via the experiment at the e^-e^- collision option, where dimension five operator of $e^-e^-\phi^+\phi^+$, which is the sub-diagram of the loop diagrams for neutrino mass matrix. This direct test of the dimension five operator is essential to identify the radiative seesaw models.

The Majorana nature in the Zee–Babu model is in the lepton number violating coupling constant μ of $k^{++}\omega^-\omega^-$, which generates the dimension five operator of $e^-e^-\omega^+\omega^+$ at the tree level via the s-channel k^{--} exchange diagram. The cross section of $e^-e^- \to \omega^-\omega^-$ is given by

$$\sigma\left(e^-e^- \to \omega^-\omega^-\right) = \frac{1}{8\pi}\sqrt{1-\frac{4m_\omega^2}{s}}\,\frac{\mu^2 g_{ee}^2}{(s-m_k^2)^2 + m_k^2\Gamma_k^2}, \qquad (14)$$

where the total width Γ_k of $k^{\pm\pm}$ is computed as about 168 GeV in our scenario in Eq. (11). On the other hand, in the Ma model and the AKS model, the operator comes from the t-channel right-handed neutrino exchange diagram. The cross section is evaluated as

$$\sigma\left(e^-e^- \to \phi^-\phi^-\right) = \int_{t_{\min}}^{t_{\max}} dt\,\frac{1}{128\pi s}\left|\sum_{\alpha=1}^{n}\left(|c^\alpha|^2 m_{N_R^\alpha}\right)\left(\frac{1}{t-m_{N_R^\alpha}^2} + \frac{1}{u-m_{N_R^\alpha}^2}\right)\right|^2, \qquad (15)$$

where n is the number of generation of right-handed neutrinos, ϕ^- represents the Z_2-odd charged scalar boson ξ^- in the Ma model and S^- in the AKS model. The constants c^α represent $\hat{h}_e^\alpha$ or h_e^α in the Ma model or the AKS model, respectively. We note that due to the Majorana nature of the t-channel diagram, we obtain much larger cross section in the e^-e^- collision than in the e^+e^- collision in each model assuming the same collision energy.

The mass matrix of left-handed neutrinos is generated at the one, two and three loop levels in the Ma model, the Zee–Babu model and the AKS model, respectively. Therefore, the coupling constants can be basically hierarchical among the models, so are the cross sections. For the typical scenarios in these models, the cross sections are shown in Fig 5. The rate of $\omega^-\omega^-$ in the Zee–Babu model can be larger than several times 100 fb for 800 GeV $\lesssim \sqrt{s} \lesssim$ 1.5 TeV. It becomes maximal (several times pb)

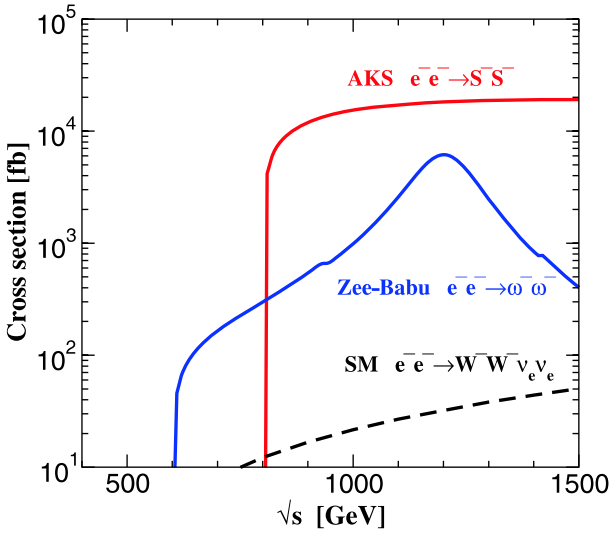

Fig. 5. The cross sections of like-sign charged Higgs pair productions in the Zee–Babu model ($\omega^-\omega^-$) and in the AKS model (S^-S^-) are shown as a function of the collision energy $\sqrt{s}$. The parameters in the Zee–Babu and the AKS model are taken as in Eq. (11) and Eq. (13), respectively.

at $\sqrt{s} \sim m_k$, and above that asymptotically reduces by $1/s$. The maximal value of the cross section is sensitive to the value of g_{ee} and μ. In the parameter sets where these coupling constants are smaller the cross section becomes smaller. The signal should be like-sign dilepton with a missing energy. On the other hand, in the Ma model, production cross sections of $e^-e^- \to \xi^-\xi^-$ are smaller than 10^{-4} fb because the coupling constants $\hat{h}_i^\alpha$ are very small in the parameters in Eq. (12). Allowing some fine tuning, $\hat{h}_i^\alpha$ may be at most 0.01 for heavier N_R^α. In any case, the cross section of $e^-e^- \to \xi^-\xi^-$ is smaller than 10^{-3} fb. Hence, most of the successful scenarios in the Ma model the process $e^-e^- \to \xi^-\xi^-$ is difficult to be seen. In the AKS model, the cross section of $e^-e^- \to S^-S^-$ is large, and its value amounts to about 15 pb at $\sqrt{s} = 1$ TeV in the scenario given in Eq. (13). Above the threshold, the magnitude of the cross sections are not sensitive to $\sqrt{s}$, so that even if $m_{S^\pm}$ would be at the TeV scale, we might be able to test it at future multi-TeV linear colliders, such as the Compact Linear Collider [35]. Because $B(S^\pm \to \eta^0 H^\pm) \simeq B(H^\pm \to \tau^\pm \nu) \simeq 100\%$, the signal should be $\tau^-\tau^-\nu\nu\eta\eta$ with almost the same rate as long as $m_{S^\pm} < m_{N_R^\alpha}$.

The background mainly comes from $W^-W^-\nu_e\nu_e$, and the cross section is about 2.3 fb (22 fb) for $\sqrt{s} = 500$ GeV (1 TeV). The branching ratio for the leptonic decay of W bosons is 30%, so that the rate of the final state $\ell\ell'\nu\nu\nu\nu$ is at most 2 fb or less. Therefore, the signal in the AKS model and in the Zee–Babu model can be seen.

Apart from the TeV-scale radiative seesaw models, there are many models with lepton number violating interactions or right-handed Majorana neutrinos. Atwood et al. have discussed the signature of heavy Majorana neutrinos in the model without Z_2 symmetry via charged Higgs pair production at e^+e^- and e^-e^- collisions [36].[10] In supersymmetric models, Majorana particles also appear, and their effects also give similar t-channel contributions to the above models in the slepton pair production through the gauge couplings, $e^-e^- \to \tilde{e}^-\tilde{e}^-$, whose cross section is of $\mathcal{O}(100)$ fb. The final state would be $e^-e^-\chi^0\chi^0$ for example.

The e^-e^- collision experiment is useful to test the Majorana nature of radiative seesaw models such as the Zee–Babu model and the AKS model via like-sign pair production of charged scalar bosons. The cross section can be significant and hierarchical among these models. The signal can be observed as a model dependent final state, by which we can discriminate the models. Although in this Letter we did not explicitly discuss the KNT model that also contains TeV-scale right-handed neutrinos N_R^α, we found that the cross section of $e^-e^- \to S_2^-S_2^-$ (S_2^- is the Z_2-odd isosinglet charged scalar boson) is very small because the coupling constants for $\bar{e}_R N_R^\alpha S_2^-$ ($\alpha = 1, 2$) are tiny [12].

5. Conclusion

We have discussed general features of TeV-scale radiative seesaw models. They are characterized by an extended scalar (Higgs) sector and the Majorana nature. We have mainly discussed the concrete models with neutrino mass generation at one-loop (the Ma model), two-loop (the Zee–Babu model), and at three-loop (the model in Ref. [6]). Various phenomenological aspects of these models have been discussed especially in experiments at the LHC and at the ILC. We have found that, while the extended Higgs sector can be explored at the LHC, the Majorana nature of the models can directly be tested at the ILC via the pair production of the charged scalar bosons at the electron–positron and electron–electron collision experiments. The detailed realistic simulation has to be done elsewhere.

Acknowledgements

We like to thank Ernest Ma for useful discussions. The work of S.K. was supported, in part, by Grant-in-Aid for Scientific Research (C), Japan Society for the Promotion of Science (JSPS), No. 19540277.

References

[1] T. Yanagida, in: Proceedings of Workshop on the Unified Theory and the Baryon Number in the Universe, KEK, Tsukuba, Japan, 1979, p. 95;
M. Gell-Mann, P. Ramond, R. Slansky, in: Proceedings of Workshop Supergravity, Stony Brook, New York, 1979, p. 315.
[2] A. Zee, Phys. Lett. B 93 (1980) 389;
A. Zee, Phys. Lett. B 95 (1980) 461, Erratum;
A. Zee, Phys. Lett. B 161 (1985) 141.
[3] A. Zee, Nucl. Phys. B 264 (1986) 99;
K.S. Babu, Phys. Lett. B 203 (1988) 132.
[4] L.M. Krauss, S. Nasri, M. Trodden, Phys. Rev. D 67 (2003) 085002.
[5] E. Ma, Phys. Rev. D 73 (2006) 077301.
[6] M. Aoki, S. Kanemura, O. Seto, Phys. Rev. Lett. 102 (2009) 051805.
[7] E. Ma, Phys. Lett. B 662 (2008) 49;
E. Ma, Mod. Phys. Lett. A 23 (2008) 721;
R.A. Porto, A. Zee, Phys. Rev. D 79 (2009) 013003;
E. Ma, D. Suematsu, Mod. Phys. Lett. A 24 (2009) 583;
T. Hambye, K. Kannike, E. Ma, M. Raidal, Phys. Rev. D 75 (2007) 095003.
[8] S.T. Petcov, Phys. Lett. B 115 (1982) 401;
S. Kanemura, T. Kasai, G.L. Lin, Y. Okada, J.J. Tseng, C.P. Yuan, Phys. Rev. D 64 (2001) 053007.
[9] K.S. Babu, C. Macesanu, Phys. Rev. D 67 (2003) 073010.
[10] D. Aristizabal Sierra, M. Hirsch, JHEP 0612 (2006) 052.
[11] M. Nebot, J.F. Oliver, D. Palao, A. Santamaria, Phys. Rev. D 77 (2008) 093013.
[12] K. Cheung, O. Seto, Phys. Rev. D 69 (2004) 113009.
[13] J. Kubo, E. Ma, D. Suematsu, Phys. Lett. B 642 (2006) 18;
D. Aristizabal Sierra, J. Kubo, D. Restrepo, D. Suematsu, O. Zapata, Phys. Rev. D 79 (2009) 013011;
D. Suematsu, T. Toma, T. Yoshida, Phys. Rev. D 79 (2009) 093004.
[14] M. Aoki, S. Kanemura, O. Seto, Phys. Rev. D 80 (2009) 033007.
[15] N.G. Deshpande, E. Ma, Phys. Rev. D 18 (1978) 2574.

[10] Recently, charged Higgs pair production at e^-e^- collider is studied in a specific model with three TeV-scale right-handed neutrinos and four Higgs doublets in Ref. [37].

[16] R. Barbieri, L.J. Hall, V.S. Rychkov, Phys. Rev. D 74 (2006) 015007.
[17] Q.H. Cao, E. Ma, G. Rajasekaran, Phys. Rev. D 76 (2007) 095011.
[18] E. Lundström, M. Gustafsson, J. Edsjö, Phys. Rev. D 79 (2009) 035013.
[19] L. Lopez Honorez, E. Nezri, J.F. Oliver, M.H.G. Tytgat, JCAP 0702 (2007) 028.
[20] M. Aoki, S. Kanemura, K. Tsumura, K. Yagyu, Phys. Rev. D 80 (2009) 015017.
[21] H.S. Goh, L.J. Hall, P. Kumar, JHEP 0905 (2009) 097.
[22] S. Su, B. Thomas, Phys. Rev. D 79 (2009) 095014.
[23] H.E. Logan, D. MacLennan, Phys. Rev. D 79 (2009) 115022.
[24] A. Belyaev, R. Guedes, S. Moretti, R. Santos, arXiv:0912.2620 [hep-ph].
[25] G. Passarino, M.J.G. Veltman, Nucl. Phys. B 160 (1979) 151.
[26] V.D. Barger, J.L. Hewett, R.J.N. Phillips, Phys. Rev. D 41 (1990) 3421.
[27] Y. Grossman, Nucl. Phys. B 426 (1994) 355.
[28] S. Kanemura, Y. Okada, E. Senaha, Phys. Lett. B 606 (2005) 361.
[29] G. Aad, et al., The ATLAS Collaboration, arXiv:0901.0512 [hep-ex].
[30] B. Di Girolamo, L. Neukermans, Atlas Note ATL-PHYS-2003-006, 2003;
M. Warsinsky, ATLAS Collaboration, J. Phys. Conf. Ser. 110 (2008) 072046.
[31] J.F. Gunion, C. Loomis, K.T. Pitts, in: Proceedings of 1996 DPF/DPB Summer Study on New Directions for High-Energy Physics (Snowmass 96), Snowmass, Colorado, 25 Jun–12 Jul 1996, p. LTH096, arXiv:hep-ph/9610237.
[32] A.G. Akeroyd, M. Aoki, Phys. Rev. D 72 (2005) 035011.
[33] M. Schumacher, Report No. LC-PHSM-2003-096.
[34] A. Pukhov, et al., arXiv:hep-ph/9908288;
A. Pukhov, arXiv:hep-ph/0412191.
[35] E. Accomando, et al., CLIC Physics Working Group, arXiv:hep-ph/0412251.
[36] D. Atwood, S. Bar-Shalom, A. Soni, Phys. Rev. D 76 (2007) 033004.
[37] W. Grimus, L. Lavoura, Phys. Lett. B 687 (2010) 188.